Effect of Nanotube Functionalization on the Properties of Single-Walled Carbon Nanotube/Polyurethane Composites

FABIAN BUFFA,[1] GUSTAVO A. ABRAHAM,[1] BRIAN P. GRADY,[2] DANIEL RESASCO[2]

[1]Instituto de Investigaciones en Ciencia y Tecnología de Materiales, INTEMA (UNMdP-CONICET), Av. J. B. Justo 4302, B7608FDQ Mar del Plata, Argentina

[2]School of Chemical, Biological and Materials Engineering and Carbon Nanotube Technology Center (CANTEC), University of Oklahoma, 100 East Boyd, Norman, Oklahoma 73019

Received 25 September 2006; revised 21 November 2006; accepted 22 November 2006
DOI: 10.1002/polb.21069
Published online in Wiley InterScience (www.interscience.wiley.com).

ABSTRACT: A commercially available aliphatic thermoplastic polyurethane formulated with a methylene bis(cyclohexyl) diisocyanate hard segment and a poly(tetramethylene oxide) soft segment and chain-extended with 1,4-butanediol was dissolved in dimethylformamide and mixed with dispersed single-walled carbon nanotubes. The properties of composites made with unfunctionalized nanotubes were compared with the properties of composites made with nanotubes functionalized to contain hydroxyl groups. Functionalization almost eliminated the conductivity of the tubes according to the conductivity of the composites above the percolation threshold. In most cases, functionalized and unfunctionalized tubes yielded composites with statistically identical mechanical properties. However, composites made with functionalized tubes did have a slightly higher modulus in the rubbery plateau region at higher nanotube fractions. Small-angle X-ray scattering patterns indicated that the dispersion reached a plateau in the unfunctionalized composites that was consistent with the plateau in the rubbery plateau region. The room-temperature modulus and tensile strength increase was proportionally higher than almost all increases seen previously in thermoplastic polyurethanes; however, the increase was still an order of magnitude below what has been reported for the best nanotube–polymer systems. Nanotube addition increased the hard-segment glass transition temperature slightly, whereas the soft-segment glass transition was so diffuse that no conclusions could be drawn. Unfunctionalized tubes suppressed the crystallization of the hard segment; whereas functionalized tubes had no effect. J Polym Sci Part B: Polym Phys 45: 490–501, 2007
Keywords: crystallization; glass transition; nanocomposites; polyurethanes; segmented polyurethanes; SAXS; single-walled carbon nanotubes

INTRODUCTION

Thermoplastic polyurethanes belong to a class of polymers termed *thermoplastic elastomers*. Thermoplastic elastomers have the ability to stretch and return to almost their original shape, though not nearly to the degree of crosslinked elastomers. The advantage of thermoplastic elastomers over conventional elastomers is that the former can be melt-processed on conventional melt-processing equipment such as extruders. Thermoplastic polyurethanes are multiblock copolymers having the general repeat unit structure $(A_mB_n)_p$. As with all multiblock thermoplastic elastomers, one of the block units is above its glass transition temperature (T_g) at use temperature (the soft

Correspondence to: B. P. Grady (E-mail: bpgrady@ou.edu)
Journal of Polymer Science: Part B: Polymer Physics, Vol. 45, 490–501 (2007)

segment), and the other is below its T_g (the hard segment). Through changes in the individual block characteristics such as the molecular weight and chemical identity, polyurethanes can be made to be hard or soft. Polyurethanes are well known for being extremely tough; that is, they extend to rather large elongations and have rather high tensile strengths. Thermoplastic polyurethanes are used widely in many industries, including a variety of medical devices,[1] sporting goods, and clothing.[2]

The flexibility of polyurethane chemistry translates into substantial flexibility in terms of polyurethane polymer physics. For example, in a single sample, it is possible to have a soft-segment glass transition, a soft-segment melting point, a hard-segment glass transition, and a hard-segment melting point. The purpose of this article is to measure the changes in the various mechanical, electrical, thermal, and morphological parameters with the addition of single-walled carbon nanotubes to a particular polyurethane, and the complexity of polyurethane morphology and chemistry makes this a very difficult task.

There are two main types of carbon nanotubes: multiwalled nanotubes (MWNTs), which are composed of concentric tubes having many different radii, and single-walled nanotubes (SWNTs). The diameters of carbon nanotubes vary from 1.4 to 100 nm for MWNTs and from 0.4 to 3 nm for SWNTs with an aspect ratio of 1000 or more. The moduli for MWNTs and SWNTs are approximately 270 GPa and 1 TPa, respectively, whereas the tensile strengths are 11 and 200 GPa, respectively.[3] The fact that the electrical properties of SWNTs are much better than those of MWNTs, and the fact that the inner walls of MWNTs do not contribute significantly to the mechanical properties of the materials, can make SWNTs more attractive to researchers. Single-walled carbon nanotubes, besides their superb mechanical properties, also have excellent electrical properties: the conductivity is 5 times that of copper. The thermal conductivity of SWNTs is also extremely high, higher than that of diamond or copper. Such properties suggest that nanotubes should be excellent materials for incorporation with polymers. Not surprisingly, a large number of studies have been performed during the last 10 years on nanotube–polymer composites.

The dispersion of the nanotubes in the polymer is a key issue. With polyurethanes, there are essentially three ways to disperse nanotubes in a polymer: (1) melt mixing; (2) the dispersion of the tubes in a solvent and dissolution of the polymer in the same solvent, followed by solvent evaporation; and (3) the reaction of the monomers or prepolymer (most thermoplastic polyurethanes are made by a two-step process) in the presence of dispersed nanotubes. To our knowledge, the former has not been attempted, presumably because of how poorly melt mixing tends to disperse tubes and because the latter method is industrially practical. The latter method was used to produce MWNT–polyurethane composites;[4] first isophorone diisocyanate was reacted with poly(tetramethylene oxide) (PTMO) in an organic solvent, then this mixture was emulsified in water, and to it a water solution containing dispersed nanotubes was added. Ethylenediamine was added as a chain extender to react with the terminal isocyanate groups. The percolation threshold was extremely low, approximately 0.1 wt %, indicative of an excellent nanotube dispersion. The same waterborne prepolymer approach was used with functionalized nanotubes that could react with the prepolymer.[5] In a similar but different approach, nanotubes were first dispersed in the liquid soft segment, and then the reaction was performed in one step; that is, this mixture was added to the isocyanate, methylene diisocyanate (MDI), and chain extender, 1,4-butanediol (BDO), at one time.[6] Soft-segment chains were also attached to the nanotubes before dispersion in the soft segment.[7,8] In another variation, an MDI/PTMO prepolymer was chain-extended with functionalized MWNTs.[9]

Solution mixing, which often produces the most well-dispersed nanotube–polymer composites, has been used to mix nanotubes and polyurethanes. Vaia and coworkers[10,11] used tetrahydrofuran (THF) to mix MWNTs into a commercial polyurethane with a polyester soft segment and aromatic hard segment and achieved a percolation threshold of 0.5 vol %. THF was also used with a commercial polyurethane, whose chemical composition was not identified, and through controlled evaporation was able to drive SWNT alignment.[12,13] Dimethylformamide (DMF) was used with an MDI/BDO polyester to produce electrospun fibers filled with SWNTs.[14] Finally, mixed THF and DMF were used to cast MDI/BDO/PCL polyurethanes into films for electroactuator testing.[15]

The purpose of this article is to investigate the effect of nanotubes on a particular polyur-

ethane. This study differs substantially from previous studies, in that this polyurethane consists of a nonaromatic hard segment, and the hard-segment level is much higher than that explored previously. Nanotubes were also functionalized to contain hydroxy groups to presumably enhance the interaction with the urethane groups via hydrogen bonding and compared to the nonfunctionalized tubes.

EXPERIMENTAL

Materials

The selected solution-grade aliphatic polyurethane (Tecoflex hardness: 60 Shore D) was provided by Thermedics, Inc. (Massachusetts). This material contained a methylene bis(cyclohexyl) diisocyanate (HMDI) hard segment and a PTMO soft segment (molecular weight = 1000 g/mol) and was chain-extended with BDO. DMF, 1,2-dichlorobencene, 4-(1-hydroxyethyl)aniline (HEA), acetonitrile, isoamyl nitrite, and 2-propanol were provided by Aldrich and were used as received. Purified CoMoCAT single-walled carbon nanotubes were provided by Southwest Nanotechnologies (Norman, Oklahoma).

Functionalization of SWNTs

Functionalization followed a methodology similar to that established by Tour and coworkers.[16,17] In a typical experiment, a 20-mg (1.67-mmol) sample of SWNT was bath-sonicated for 2 h in 25 mL of *o*-dichlorobenzene. The resulting suspension was placed in a two-necked, round-bottom glass flask together with a solution of 3.34 mmol of HEA in 10 mL of acetonitrile. With a reflux condenser in one of the flask necks, the mixture was stirred for 10 min with bubbling nitrogen. Next, 5.12 mmol of isoamyl nitrite was added to the mixture, which was then heated to 60 °C and kept at this temperature for 15 h, under continuous stirring. After cooling to 35–45 °C, the mixture was diluted with 75 mL of DMF and filtered through a PTFE membrane (0.2-μm pore size). The solid retentate was first washed with copious amounts of DMF and then further washed in sequential cycles of sonication in 2-propanol (2 h each) followed by filtration until the liquid filtrate came out colorless. The resulting purified solid was vacuum-dried overnight at room temperature.

Optical Absorption

Functionalized and unfunctionalized samples were analyzed by optical absorption in DMF suspensions. The suspensions were prepared by horn-sonication of the SWNT samples in DMF (0.01 mg/mL) for 15–30 min. The UV–vis absorption spectra were obtained with a Shimadzu UV-2101PC scanning spectrophotometer.

Preparation of the Polyurethane–SWNT Composites

For the polyurethane–SWNT films, several mixtures were prepared with various amounts of SWNTs (both functionalized and unfunctionalized). The different SWNT concentrations used in the series were 0.1, 0.3, 0.5, 1.0, 1.8, and 2.6 wt % with respect to the final SWNT/polyurethane mixture. In a typical preparation, a predetermined amount of SWNT was bath-sonicated for 2 h in 15 mL of DMF. A fixed amount of polyurethane (pellets) was added to this suspension under continuous sonication and left under sonication for an extra 1 h to readily solubilize the polyurethane. Subsequently, the mixture was poured over a Petri dish containing a silicone bed, which provided a smooth uniform surface and facilitated the detachment of the film at the end of the process. The Petri dish was then placed in an oven at 60 °C and left overnight to complete the evaporation of the solvent.

Raman Spectroscopy

Raman spectra were obtained in a Jovin Yvon-Horiba LabRAM HR-800 equipped with a charged-coupling-device detector and with three different laser excitation sources having wavelengths of 633 nm (He–Ne laser) and 514 and 488 nm (Ar laser).

Differential Scanning Calorimetry (DSC)

DSC experiments were carried out on a TA Instruments Q-1000. To ensure good sample-pan contact, the sample was melted before the testing. The sample was melted at 190 °C and held there for 5 min, then cooled at 20 °C/min to −140 °C, then heated at 10 °C/min to 200 °C, and finally cooled at 20 °C/min to room temperature. The samples were then allowed to anneal at room temperature for 9 days, and then a second heating scan was run. Indium, tin, biphenyl, and cyclopentane were used as temperature stand-

ards, indium was used as an enthalpy standard, whereas the heat capacity was calibrated with a sapphire encapsulated in a DSC sample pan.

Tensile Tests

Tensile tests were measured with an ASTM D 1708 dog-bone die on a United STM-2K tensile tester at the rate of 5 mm/min. In most cases, at least three samples were tested, and the error bars represented the standard deviation of the measurement.

Dynamic Mechanical Analysis (DMA)

DMA on a Rheometric Scientific RSA II in tension was used to measure the storage modulus (E') and loss modulus (E'') of thin films (ca. 0.1 mm) in tension. Temperature steps of 3–4 °C were used, and the samples were measured at a frequency of 1 Hz. Static force tracking dynamic force was used to account for the change in the stiffness with the temperature.

Conductivity Measurements

Electrical conductivities were tested by a two-point-probe method with a specially constructed resistivity chamber, which was calibrated by a Keithley 610C electrometer and Keithley 8009 test fixture. The lower limit of this chamber was approximately 1×10^{-14} S/cm; this chamber was used because it required much less sample than the Keithley 8009 fixture. Good electrical contact between the gold electrodes and the sample was ensured by compressive pressure applied by screws.

Wide-Angle X-Ray Scattering (WAXS) and Small-Angle X-Ray Scattering (SAXS)

WAXS patterns were collected at room temperature with a Bruker AXS D8 Discover system with a 2D wire detector. The samples were measured in symmetric transmission; two different source-detector angles were used, and the data were combined by the matching of the intensities in the overlap region. No angular correction was performed for the dependence of the sample absorption on the scattering angle for a given source-detector angle; the transmittance of all samples was fairly high (~90%), and no distortions were apparent in the overlap region. A measured transmittance was not used to subtract the background spectra from the sample spectra; rather, the transmittance was set at a value that gave a flat background.

SAXS patterns were collected on an Osmic Micro Max system for SAXS. A 10 cm × 10 cm wire detector was placed approximately 150 cm from the sample position, and silver behenate was used to determine the exact pixel-to-q conversion ($q = 4\pi\sin\theta/\lambda$; $\theta = 0.5 \times$ scattering angle; $\lambda = 1.54$ Å). The patterns were corrected for dark current, pixel-to-pixel variations in the detector sensitivity, and background scattering with the measured sample transmittance. 2D patterns were then circularly averaged and converted to absolute intensities with a calibrated high-density polyethylene sample.

RESULTS AND DISCUSSION

The presence of functional groups on the nanotube walls was clearly demonstrated by Raman spectroscopy and optical absorption. Figure 1 compares the Raman spectra of functionalized and unfunctionalized nanotubes with an excitation laser with a wavelength of 633 nm. As previously observed, a pronounced difference in the relative intensity of the D band (1290 cm^{-1}) with respect to the main G band is clearly evident. The increase in the D band has been previously reported[18] and used as an indication of covalent side-wall functionalization, as it reflects the conversion of the hybridization of some C atoms on the nanotube wall from sp^2 to sp^3. Also, the UV–vis absorption spectra of the func-

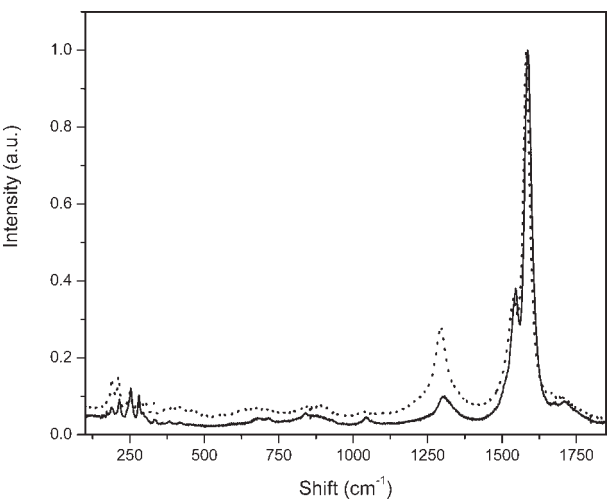

Figure 1. Raman spectra (633-nm excitation) of (—) SWNTs and (· · ·) HEA-functionalized nanotubes.

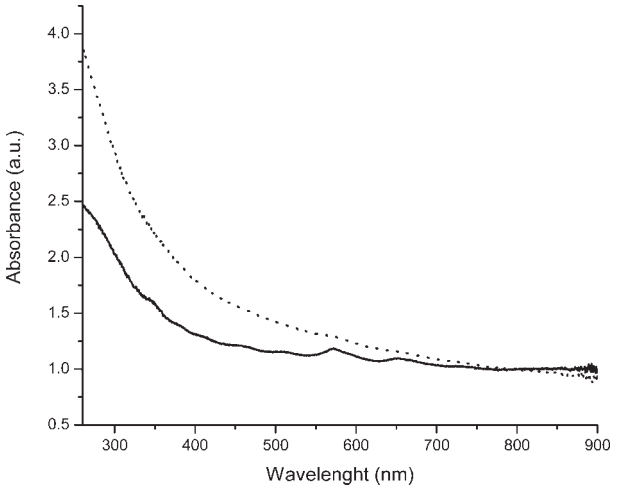

Figure 2. Absorption spectra in DMF of (—) pristine SWNTs and (· · ·) HEA-functionalized nanotubes suspended in DMF.

tionalized SWNTs (Fig. 2) show the disappearance of the typical bands appearing near 660 and 566 nm, which correspond to the S22 transitions of the (6,5) and (7,5) nanotubes, which constitute the majority of the semiconducting nanotubes present in the CoMoCAT material.[19,20]

The conductivity of the nanotube composites is shown graphically in Figure 3. The percolation threshold for both materials is between 0.5 and 1%; only three concentrations had a measurable conductivity with our apparatus, and these are not enough data points to accurately fit the two-parameter scaling law necessary to determine the percolation threshold. Functionalization clearly significantly reduced the ability of the nanotube composites to conduct electricity. Because other properties of the composites containing functionalized tubes are about the same for those containing unfunctionalized tubes, the drop in conductivity shown in Figure 3 with functionalized tubes is due to the inherent conductivity drop of the tubes themselves rather than increased agglomeration with the functionalized tubes. In general then, the dispersion, as measured by electrical percolation, is good, but not as good as the best values found for other systems.

The addition of nanotubes causes a monotonic rise in both the Young's modulus (E) and E', as shown in Figure 4. The increase in the modulus is approximately 25% for each 1% increase in the nanotube concentration. However, as also shown in Figure 4, the rise is quite small in comparison with the rise that would be expected

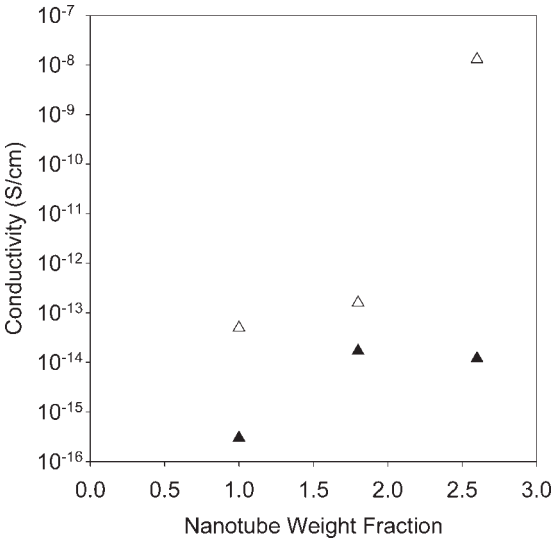

Figure 3. Conductivity of composites made from (▲) functionalized and (△) unfunctionalized nanotubes. The lower limit of measurable conductivity for our device was 10^{-16} S/cm.

according to the mixing law[21] shown here:

$$E_{composite} = (1 - V_f)^* E_{polymer} + 0.2^* V_f^* E_{fiber} \quad (1)$$

where V_f is the volume fraction of nanotubes. Equation 1 is applicable to randomly oriented fibers, and a carbon nanotube modulus of 1 TPa[22] and a polymer density of 1.1 g/cm^3 are

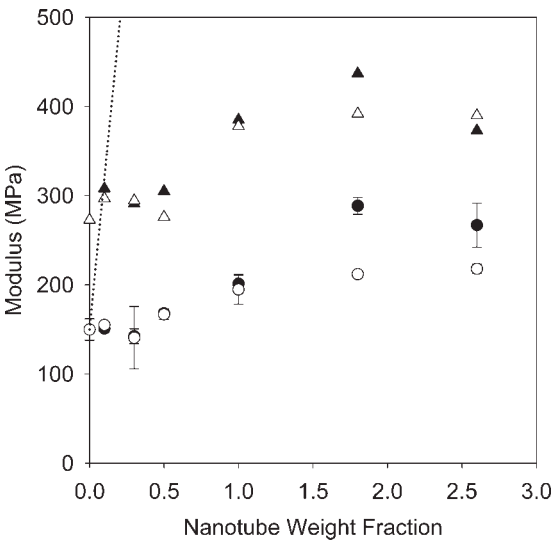

Figure 4. Moduli of composites made from (▲,●) functionalized and (△,○) unfunctionalized nanotubes. The circles represent E, whereas the triangles represent E' at room temperature. The dotted line represents the E values that would be expected from a simple rule of mixing.

Table 1. Comparison of the Mechanical Properties of Nanotube-Filled Polyurethanes

Nanotube Type	Reference	Mixing Procedure	E of Pure Polyurethane (MPa)	$dE_{composite}/d\phi_{nanotube}$ (GPa)	Tensile Strength/ Tensile Strength Matrix at ~1% Tubes
MWNT-functional	5	Waterborne solvent mixing, prepolymer	5	2.5	2
SWNT	12,13	Solvent	7.7[a]	1.4[a]	1.2 (0.5)
MWNT-functional	9	Acid on MWNT directly incorporated into the polyurethane prepolymer	3	0.1	1.1 (4)
SWNT-functional	7	Grafted SWNT mixed with the soft segment and then reacted with polyurethane	5.5	2	1.2 (0.7)
SWNT	6,7	SWNT mixed with the soft segment and then reacted with polyurethane	5.5/3.5	0.5	1.4
MWNT	6	MWNT mixed with the soft segment and then reacted with polyurethane	3.5		1.2
MWNT	4	Waterborne solvent mixing, prepolymer	10.2	0.4	1.03
MWNT-functional	4	Acid functionalization, waterborne solvent mixing with the prepolymer	10.2	1.4	1.25
MWNT	11	Solvent	12.5	0.5	0.7
SWNT	This article	Solvent	150	4	1.5

[a] In the reference, the listed units of the modulus are gigapascals. This is assumed to be a typo; this polyurethane is a material with a high soft-segment content, as evidenced by its strain at break.

assumed. Another way of looking at the efficiency of the reinforcement is to calculate the slope of the change in the modulus with the volume fraction, that is, $dE_{composite}/d\phi_{nanotube}$, and compare that to the median value for solution mixing compiled by Coleman et al.[3] in his recent review of carbon nanotube/polymer composites. The value in these nanotube–polyurethane composites is about 4 GPa, which is small compared with the median value of 112 GPa reported in that article. However, the median was calculated with both oriented and unoriented systems, and the increase in the modulus for well-oriented systems is expected to be roughly a factor of 5 higher. Table 1 shows the reinforcement efficiency for different polyurethanes tabulated from previous studies in the literature; on this basis, our reinforcement efficiency is quite good. Table 1 also shows that our material has significantly higher hard-segment contents than the other materials because the modulus is significantly higher. The strain at break values (not shown) confirm this; other authors in general have investigated polyurethanes having strain at breaks around 1000%, whereas ours has a strain at break of about 100%.

The DMA spectra shown in Figures 5 and 6 have three significant transitions: a broad peak in E'' centered around −60 °C, a peak in tan δ with a maximum intensity at about 50 °C, and finally a hard-segment melting transition around 130 °C. The broad peak around −60 °C is due to the soft-segment glass transition. The transition is small and very broad and is not accompanied by an abrupt drop in E'. Not surprisingly, a discontinuity in the heat capacity could not be seen in DSC spectra at temperatures corresponding to the soft segment glass transition temperature; further attesting to the weakness of this transition. Because of peak broadness and instrument noise, nothing could be determined regarding the peak position or magnitude with respect to the addition of nanotubes. The temperature of the transition is reasonable for polyurethanes with a PTMO soft segment, indicating that the soft-segment phase is of the purity normally associated with PTMO in polyurethanes.[23,24] The small magnitude of the soft-segment glass transition also indicates that this particular polyurethane has a high concentration of hard segments.[25]

The second feature in the DMA spectra is the drop in both E' and E'' around 50 °C and the corresponding peak in tan δ. The assignment of this feature is difficult because a soft-segment melting transition and a hard-segment glass transition can occur in this temperature region.[26] Figure 7

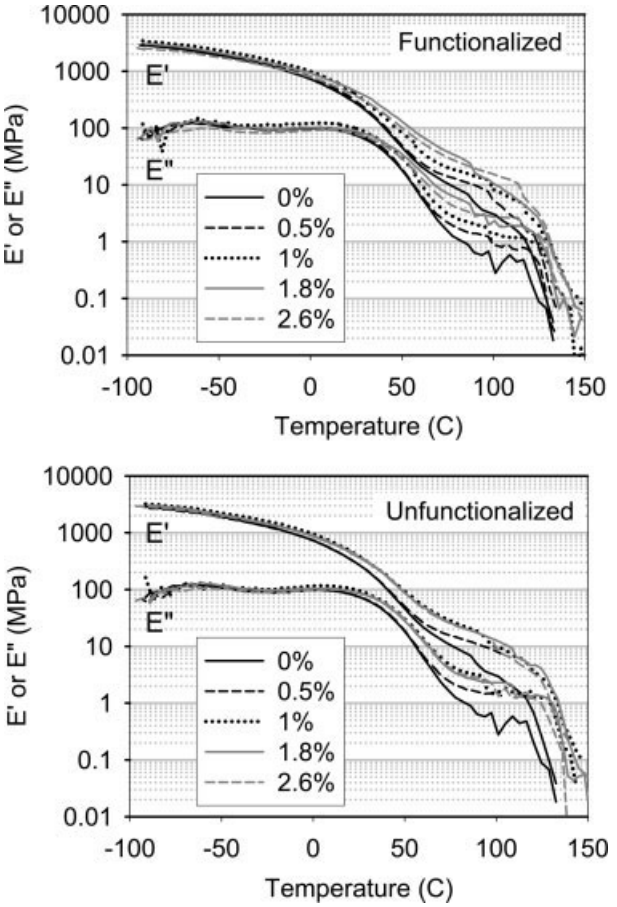

Figure 5. E' and E'' as functions of temperature for polyurethane–nanotube composites.

shows that in fact both could be occurring; DSC scans show a small and broad, but noticeable, peak that is centered around 40 °C as well as the hard-segment glass transition that occurs around 70 °C. Given the size of the peak, as well as the fact that there is no evidence of any crystalline phases in X-ray scattering (see Fig. 8), most, if not all, of this transition in DMA should be attributed to the hard-segment glass transition. As another piece of supporting information, in a study with the same hard-segment/soft-segment chain-extender combination, the soft-segment melting endotherm in DSC was many times the value here, yet the drop in E' due to melting was essentially nonmeasurable.[27]

One very interesting observation is that the height of the tan δ peak corresponding to the hard-segment T_g in the composite containing functionalized nanotubes decreases for the samples with the highest level of nanotubes. A decrease in the tan δ peak height is thought to correspond to a decrease in the amount of material participating in the transition. This change is probably either due to a decrease in the amount of the hard-segment amorphous phase or a reduction in the mobility of some chains to the point at which they do not participate in the glass transition. Such areas of restricted mobility with the same effect on the tan δ peak height have been hypothesized to occur in other thermoplastic elastomers if an immobile phase obtains a high enough local concentration.[28] Various other measurements have been performed and may help define the source of this change.

A decrease in the hard-segment amorphous phase should be measurable by the evaluation of the change in the heat capacity at the glass transition. Unfortunately, good sample-pan contact requires that samples be melted in the DSC

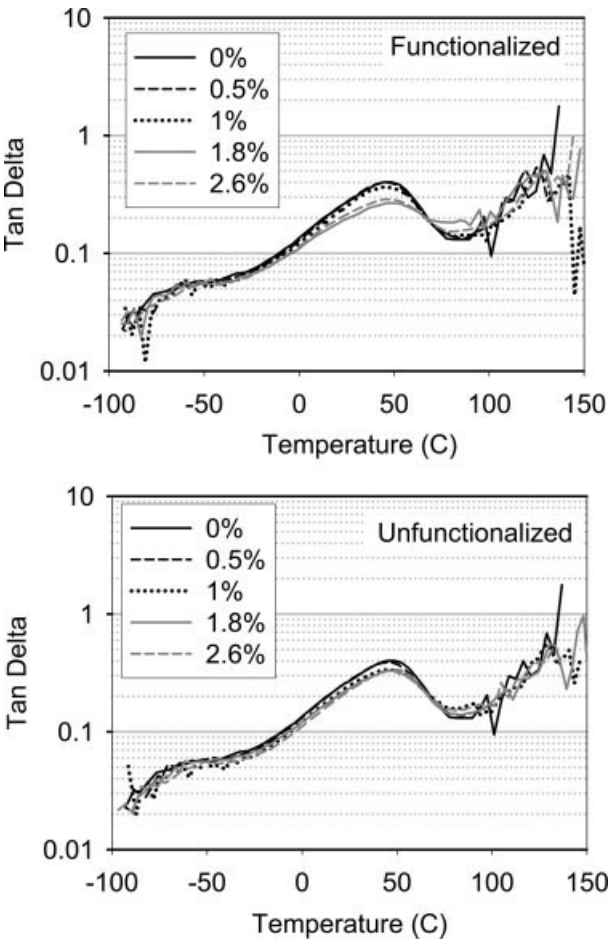

Figure 6. Tan δ as a function of temperature for polyurethane–nanotube composites. The rate of crystallization was so slow that changing the cooling rate did not yield a peak before the glass transition, even though a small peak upon heating could be seen, as shown in Figure 4.

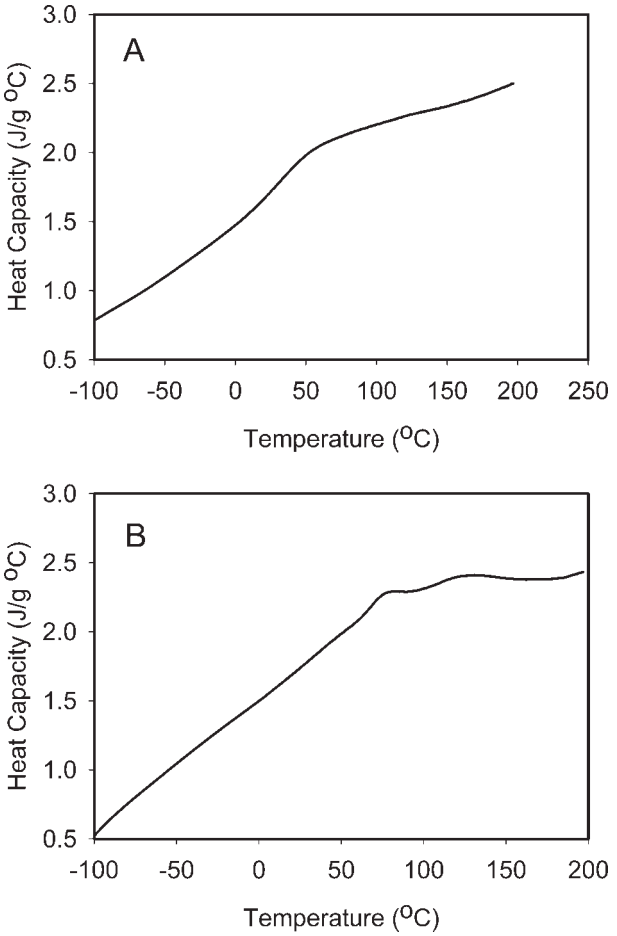

Figure 7. Representative DSC scans. This sample had a nanotube content of 0.5 wt % with unfunctionalized tubes. The top graph presents the results immediately after the sample was quench-cooled at 20 °C/min, whereas the bottom graph presents the results after annealing at room temperature for 9 days.

first, and hence the exact samples that were tested by DMA were not tested by DSC. Instead, the samples were melted and allowed to anneal at room temperature for about 9 days. Although these samples will not absolutely correspond to the DMA samples, they should relatively correspond. There is no evidence of any change in the magnitude of the heat capacity jump with increasing nanotube concentration; however, the accuracy of this procedure is not very good: sample-to-sample variation is estimated at approximately 10%. The machine accuracy is much better than 10%; the problem is in the nature of the spectra themselves. As shown in the bottom of Figure 7, the enthalpy relaxation peak corresponding to the glass transition overlaps with the hard-segment melting peak around 125 °C, and hence determining the change in the heat capacity at the glass transition reproducibly is difficult. Another possibility for the reduction in the tan δ peak size is that the hard-segment fractional crystallinity increased; unfortunately, the fractional crystallinity could not be determined either with any accuracy because of the overlap between the hard-segment glass transition and the hard-segment melting endotherm, as shown in Figure 7(A,B). Numerous efforts were attempted to at least draw a consistent baseline so that the results could be compared, but nothing was deemed satisfactory. In general, a higher crystalline fraction should yield a higher melting point, and no such trend can be seen in the DMA spectra, as shown in Figure 5. The melting

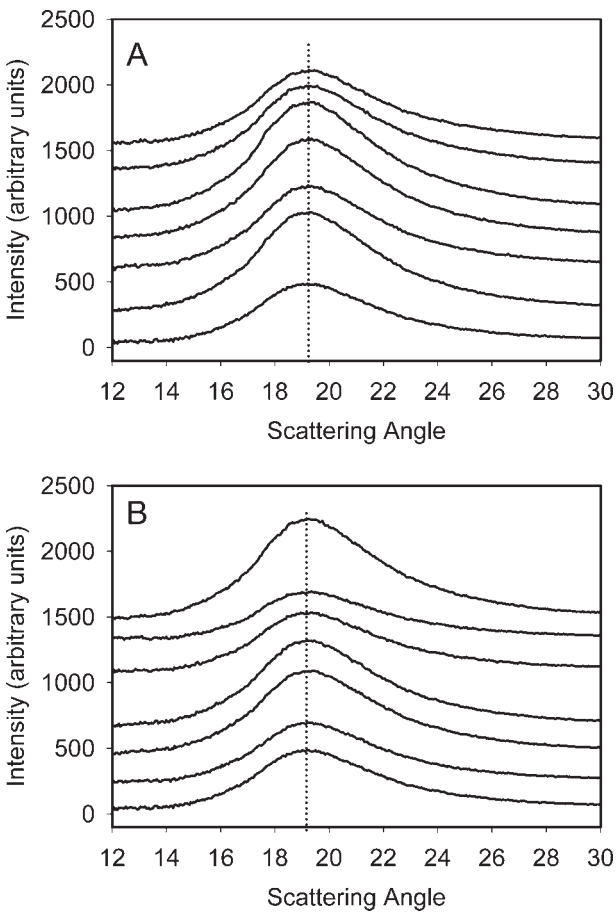

Figure 8. WAXS patterns of polyurethane–nanotube composites. The graphs have been shifted upward for clarity. The bottom graph shows functionalized nanotubes, whereas the top graph shows unfunctionalized nanotubes. From bottom to top within each graph, the nanotube concentrations are 0, 0.1, 0.3, 0.5, 1.0, 1.8, and 2.6 wt %. The dotted line has been drawn through the center of the 0% sample and is meant to show the very slight shift of the center of the amorphous halo to higher angles.

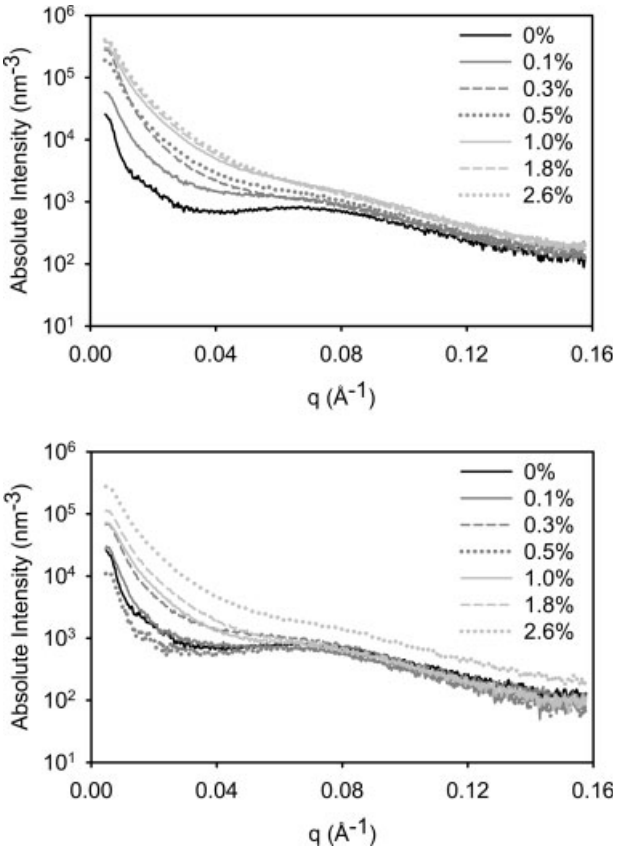

Figure 9. SAXS patterns of nanotube-filled polyurethanes. The top graph shows unfunctionalized nanotubes, whereas the bottom graph shows functionalized nanotubes.

point, or even the temperature corresponding to the peak in the melting endotherm, was also impossible to determine accurately by DSC for the samples annealed for 9 days because of the aforementioned overlap.

Another way of determining the hard-segment crystallinity is wide-angle X-ray diffraction. No peaks appear in the WAXS patterns in Figure 8, and this indicates that the crystalline structure is not well formed because an HMDI/PTMO/BDO polyurethane can show crystalline reflections.[26] In this case then, DSC is more sensitive to crystallinity than WAXS because DSC scans clearly show hard-segment melting. One interesting observation in Figure 8 shows that the amorphous halo shifts to slightly higher angles (smaller d-spacings) as the nanotube concentration increases. Because large nanotube ropes have peaks at much smaller angles than the amorphous halo,[29] the shift in the peak position is almost certainly either due to a densification of the polymer phase due to nanotube addition or, more likely, an indication that the nanotube–polymer spacing varies over a distance with an average slightly smaller than that of the polymer–polymer spacing.

The rubbery plateau region in the DMA spectra, that is, the temperature region between the glass transition of the hard segment and hard-segment melting, shows interesting E' behavior. No statistically significant difference between the moduli corresponding to functionalized and unfunctionalized tubes is found at room temperature, whereas there is a small difference at elevated temperatures. The difference at elevated temperatures occurs only at higher nanotube concentrations; E' clearly reaches a maximum value that does not increase with more nanotubes in the case of samples made with unfunctionalized tubes, whereas samples made with functionalized tubes continue to increase in modulus with increased nanotube amounts. One possibility is that the functionalized tubes have better dispersion at higher concentrations, and this difference increases the stiffness of the mobile amorphous phase that exists at high temperatures but has little effect on the already stiff and rigid amorphous phase that exists at room temperature. The other possibility is an increase in the hard-segment crystallinity; such an increase would be expected to have little effect below the T_g and have a much more significant effect above the T_g. As stated previously, there was no evidence of differences in the hard-segment crystallinity between composites made with the two tube types, although none of the evidence was conclusive because of difficulties in accurate determination.

SAXS patterns are shown in Figure 9 and confirm that at higher concentrations, functionalized tubes have better dispersion than unfunctionalized tubes. A plateau value of the background scattering at high nanotube contents is present for composites made with unfunctionalized tubes but not for composites made with functionalized tubes. The only explanation for this behavior is that the concentration of dispersed nanotubes is reaching a plateau. For example, if all aggregates were large, then a plateau would occur if the number of individually dispersed tubes were constant because large aggregates would not contribute to the background scattering. We do not favor this explanation because it is likely that such large aggregates, at least in the form of ropes, would show the characteristic diffraction peaks[29] of nanotube ropes, and these were not found (the angular

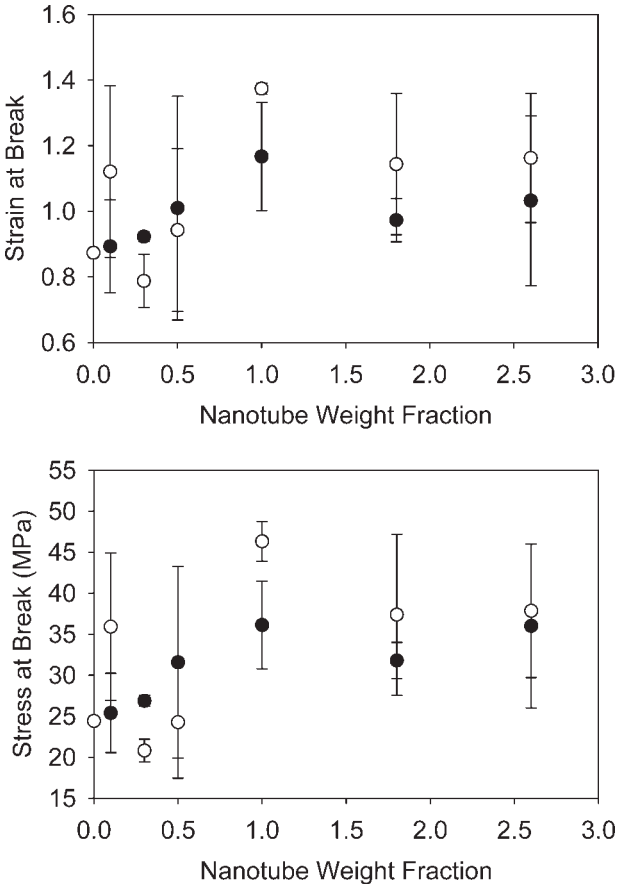

Figure 10. Ultimate mechanical properties of polyurethane–nanotube composites made from (●) functionalized and (○) unfunctionalized nanotubes.

regions in which some of these peaks exist are not shown). More likely is that the total number of dispersed tubes, whether existing as individual tubes or small ropes, is constant as the weight fraction of nanotubes increases in composites made with unfunctionalized nanotubes. In other words, in samples made with unfunctionalized tubes, the average number of tubes in a dispersed entity increases as the nanotube content increases, so the number of dispersed entities is constant. This type of behavior would yield constant background scattering intensity, but the shape would change slightly; such a change does seem to be occurring. In composites containing functionalized nanotubes, the increase in background scattering with increasing nanotube concentration indicates that the number of dispersed tubes, whether existing as individual tubes or small ropes, continues to increase as the overall nanotube concentration increases. The plateau in the background scattering with unfunctionalized tubes and no plateau with the functionalized tubes are consistent with both the plateau in the rubbery modulus and the behavior of the tan δ peak height.

The maximum around $q = 0.8$ Å^{-1}, corresponding to a Bragg spacing of about 50 Å, is at a distance characteristic of hard-segment/soft-segment phase separation. No peak at lower q normally attributed to crystalline diffraction was found; this is further evidence that crystalline phase separation is not substantial. The peak position appears to be constant with the nanotube content, although it must be emphasized that small variations would not be noticeable because of the difficulty in accurately determining the peak position on account of the increasing background scattering as nanotubes are added. Functionalized tubes have less intense background scattering than unfunctionalized tubes, and this indicates that the electron density of functionalized tubes is substantially smaller than that of unfunctionalized tubes. The reduction in the electron density is almost certainly a result of the fact that the mass density of functionalized tubes is less than the mass density of unfunctionalized tubes.

The ultimate properties from tensile measurements are shown in Figure 10. The first comment is that the error in these measurements is extremely large, much larger than is normally found for neat polymers. One likely explanation for the large error is that small agglomerated nanotubes cause micro- or even nanoscopic sample defects, which in turn cause a great deal of variability in the measured ultimate properties. Both the tensile strength and elongation at break increase with added nanotubes. Table 1 shows that the increase in the tensile strength of our samples is higher than that of all other polyurethane–nanotube composites except one. The strain at break also increases significantly; in only a few cases does the strain at break also increase with added nanotubes.[4,6,7] Also, the ultimate properties show no statistically significant difference between functionalized and unfunctionalized tubes.

Standard nonisothermal crystallization experiments were not successful in determining whether the crystallization kinetics were affected by the addition of nanotubes because the endothermic peak was not apparent before the glass transition of the hard segment. However, upon reheating, both the enthalpy and the melting temperature indicate that unfunctionalized tubes depress the crystallization rate of the

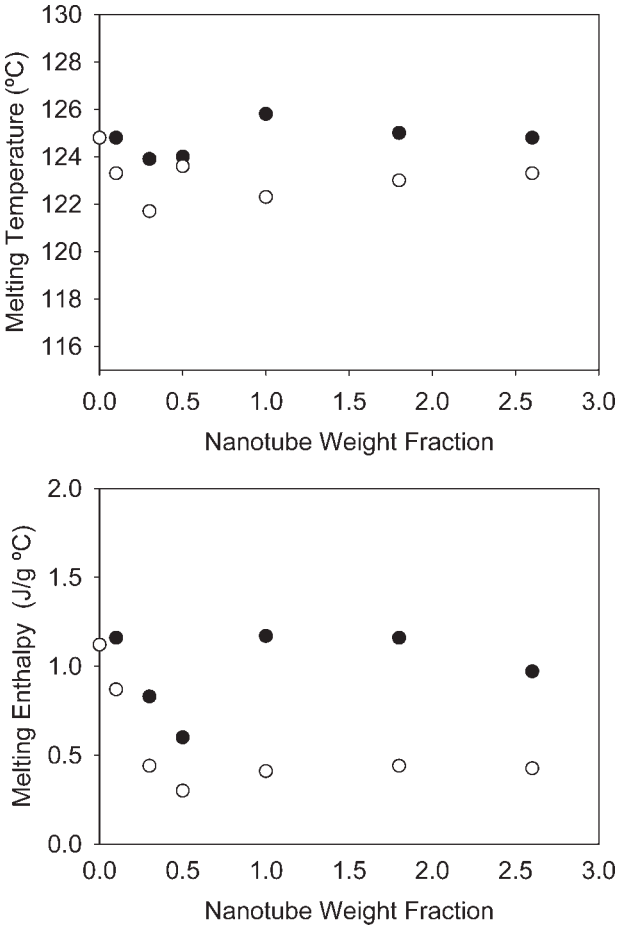

Figure 11. Properties of hard-segment crystals measured during reheating immediately after cooling from the melt at a rate of 20 °C/min to a temperature well below the soft-segment T_g. Functionalized = ●, unfunctionalized = ○.

hard segment, as shown in Figure 11, because the amount of hard-segment crystallinity and the melting temperature are reduced. It is hard to rationalize this slowing of crystallization as a nucleation effect. There are many possibilities why nanotube addition might slow crystallite growth; among these are that unfunctionalized nanotubes promote phase mixing in the melt, or unfunctionalized nanotubes are better able to prevent phase separation during cooling. In a previous study with SWNTs, it was found that tubes functionalized with soft segment had an increase in the soft-segment crystallization rate over many days, whereas there was a slight decrease, much smaller than that shown here, in the soft-segment crystallization rate with the addition of unfunctionalized tubes.[7] Functionalized tubes appear to slow the crystallization rate at low concentrations with no effect at high concentrations, and this suggests a slowing effect as well as a crystallization nucleating effect. However, nucleating effects tend to plateau very quickly at low nanotube fractions,[30,31] and this is not consistent with what is seen here. The initial slowing effect may not be real; poor sample-pan contact will give this same behavior. Regardless, it is interesting to note that the crystallization rate can be slowed by the addition of nanotubes, unlike in most cases in which nanotubes increase the crystallization rate because of a nucleating effect.[3]

A very small increase in the hard-segment T_g was found with increasing nanotube content for room-temperature-annealed samples (i.e., the DMA data and the squares in Fig. 12). In earlier studies, it was found that the soft-segment T_g decreased slightly with both SWNT and MWNT addition in an *in situ* polymerized MDI/PTMO/BDO polyurethane with a high soft-segment content. The authors attributed this finding to increased phase separation between hard and soft segments;[5,7] such behavior in our system would be consistent with the slight increase in the hard-segment T_g found. A different study found a slight increase in both the hard-segment and soft-segment T_g's;[4] this type of behavior is

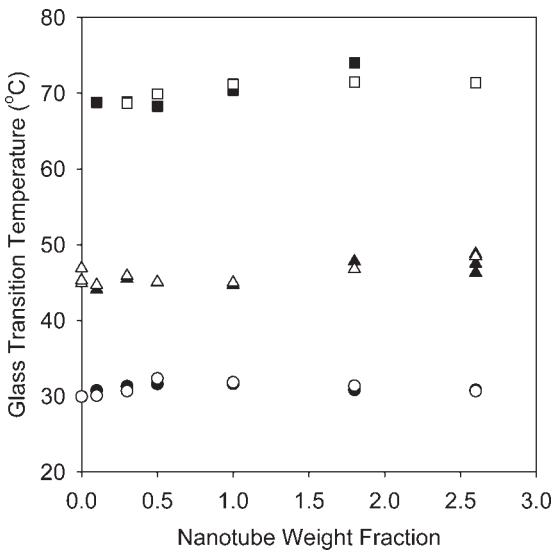

Figure 12. T_g of composites made from (■,●,▲) functionalized and (□,○,△) unfunctionalized nanotubes. The triangles represent the values determined from the location of the peak in tan δ. The circles represent the values from DSC immediately after cooling from the melt at a rate of 20 °C/min to a temperature well below the soft-segment T_g, and the squares represent the values after room-temperature annealing for 10 days.

consistent only with a modification of the polymer mobility with nanotube addition. One interesting observation is the marked change in the T_g after 9 days of room-temperature annealing; the change is almost 40 °C. There is no difference between the functionalized and unfunctionalized tubes, unlike hard-segment crystallization described earlier, which was measured over much shorter timescales. Finally, a maximum in the T_g exists as a function of the nanotube content for the samples tested immediately after cooling. A maximum suggests two competing effects; what these two competing effects are is difficult to determine.

CONCLUSIONS

The introduction of carbon nanotubes into a polyurethane with a high hard-segment content results in increases in the modulus, tensile strength, and strain at break. The increases are proportionally the highest seen in any polyurethane to date. Functionalization of the tubes leads to slightly better dispersion at high nanotube contents, although the manifestations of this improved dispersion are small. Functionalization also destroys the inherent electrical conductivity of the tubes as well. The glass transition of the hard segment increases slightly with nanotube addition, and the hard-segment crystallization rate decreases with unfunctionalized nanotube addition.

Financial support for this project was provided by a grant from the Oklahoma State Regents for Higher Education and Department of Energy (DoE-BES) grant No. DE-F602-06ER64239. The authors also thank Agencia Nacional de Promoción Científica y Tecnológica of Argentina for its partial support of this work.

REFERENCES AND NOTES

1. Lambda, N. M. K.; Woodhouse, K. A.; Cooper, S. L. Polyurethanes in Biomedical Applications; CRC: Boca Raton, FL, 1997.
2. Oertel, G. Polyurethane Handbook, 2nd ed.; Hanser: New York, 1994.
3. Coleman, J. N.; Khan, U.; Blau, W. J.; Gun'ko, Y. K. Carbon 2006, 44, 1624–1652.
4. Kwon, J.; Kim, H. J Polym Sci Part A: Polym Chem 2005, 43, 3973–3985.
5. Kuan, H. C.; Ma, C. C. M.; Chang, W. P.; Wu, H. H.; Lee, T. M. Compos Sci Technol 2005, 65, 1703–1710.
6. Xia, H.; Song, M. Soft Matter 2005, 1, 386–394.
7. Xia, H.; Song, M. J Mater Chem 2006, 16, 1843–1851.
8. Xiong, J.; Zhou, D.; Zheng, Z.; Yang, X.; Wang, X. Polymer 2006, 47, 1763–1766.
9. Jung, Y. C.; Sahoo, N. G.; Cho, J. W. Macromol Rapid Commun 2006, 27, 126–131.
10. Koerner, H.; Price, G.; Pearce, N. A.; Alexander, M.; Vaia, R. A. Nat Mater 2004, 3, 115–120.
11. Koerner, H.; Liu, W.; Alexander, M.; Mirau, P.; Dowty, H.; Vaia, R. A. Polymer 2005, 46, 4405–4420.
12. Chen, W.; Tao, X. Macromol Rapid Commun 2005, 26, 1763–1767.
13. Chen, W.; Tao, X. Appl Surf Sci 2006, 252, 3547–3552.
14. Sen, R.; Zhao, B.; Perea, D.; Itkis, M.; Hu, H.; Love, J.; Bekyarova, E.; Haddon, R. C. Nano Lett 2004, 4, 459–464.
15. Cho, J. W.; Kim, J. W.; Jung, Y. C.; Geo, N. S. Macromol Rapid Commun 2005, 26, 412–416.
16. Dyke, C. A.; Tour, J. M. Nano Lett 2003, 3, 1215–1218.
17. Bahr, J. L.; Tour, J. M. Chem Mater 2001, 13, 3823.
18. Bahr, J. L.; Yang, J.; Kosynkin, D. V.; Bronikowski, M. J.; Smalley, R. E.; Tour, J. M. J Am Chem Soc 2001, 123, 6536–6542.
19. Bachilo, S. M.; Balzano, L.; Herrera, J. E.; Pompeo, F.; Resasco, D. E.; Weisman, R. B. J Am Chem Soc 2003, 125, 11186–11187.
20. Weisman, R. B.; Bachilo, S. M. Nano Lett 2003, 3, 1235–1238.
21. Callister, W. D. Materials Science and Engineering—An Introduction, 6th ed.; Wiley: New York, 2002.
22. Wong, E. W.; Sheehan, P. E.; Lieber, C. M. Science 1997, 277, 1971–1972.
23. Wang, C.; Cooper, S. L. Macromolecules 1983, 16, 775–780.
24. Pechhold, E.; Pruckmayr, G. Rubber Chem Technol 1982, 55, 76–87.
25. Meckel, W.; Goyert, W.; Wieder, W. In Thermoplastic Elastomers, 2nd ed.; Holden, G.; Legge, N. R.; Quirk, R.; Schroeder, H. E., Eds.; Hanser: New York, 1996.
26. Nigar, M.; Blackwell, J.; Chvalun, S. N.; Seneker, S. D.; Schmelzer, H. G. Acta Polym 1996, 47, 48–54.
27. Lee, D. K.; Tsai, H. B. J Appl Polym Sci 2000, 75, 167–174.
28. Eisenberg, A.; Hird, B.; Moore, R. B. Macromolecules 1990, 23, 4098–4107.
29. Dailly, A.; Yim, J. W.; Ahn, C. C.; Miura, E.; Yazamil, R.; Fultzl, B. Appl Phys A 2005, 80, 717–724.
30. Grady, B. P.; Pompeo, F.; Shambaugh, R. L.; Resasco, D. E. J Phys Chem B 2002, 106, 5852–5858.
31. Probst, O.; Moore, E. M.; Grady, B. P.; Resasco, D. E. Polymer 2004, 45, 4437–4443.